Supporting Information

Nanofibrous bacterial cellulose-carboxymethyl cellulose composite with high wet strength and active ester-mediated stable tissue adhesion in dynamic environments

Donghyun Hwang[a], Donghyeok Kang[†a], Kiho Sung[†a] and Sungchul Shin[*ab]

[a] Department of Agriculture, Forestry, and Bioresources, Seoul National University, Seoul Republic of Korea

[b] Research Institute of Agriculture and Life Sciences, Seoul National University, Seoul, Republic of Korea

[†] These authors contributed equally: Donghyeok Kang, Kiho Sung

*Corresponding author Email: sungssc@snu.ac.kr

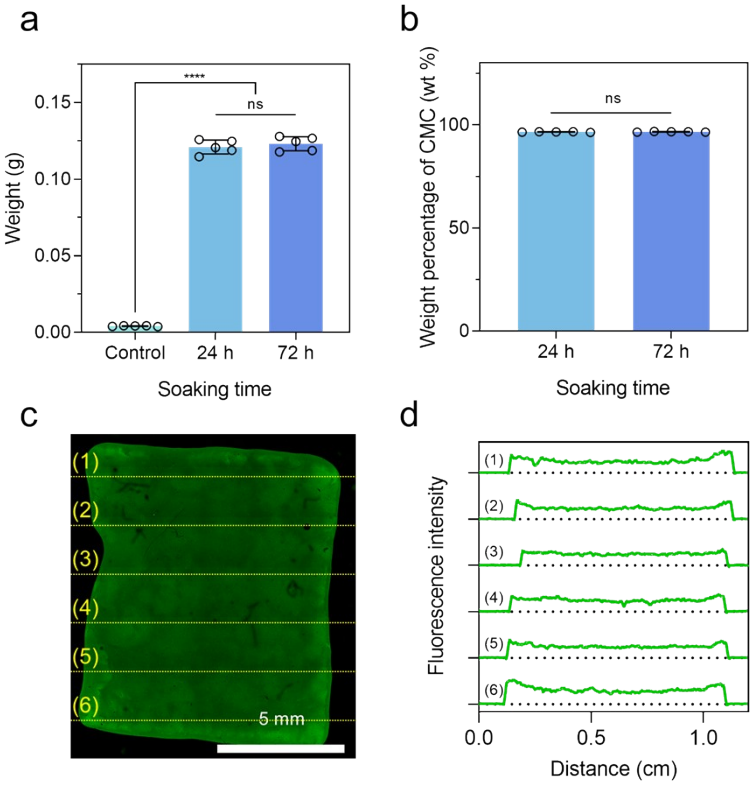

Fig. S1. Verification of CMC incorporation and spatial distribution within the BC network. (a) Dry weight of BC hydrogels after soaking in 2 wt% CMC solution for 0 h (Control), 24 h, and 72 h. Increased dry weight in the 24 h and 72 h groups indicates successful incorporation of CMC into the BC network, with no significant difference between the two soaking times. (b) Weight percentage (wt%) of CMC incorporated into the dry BC network after soaking in 2 wt% CMC solution for 24 h and 72 h. Data are presented as mean values ± SD (n = 5). No statistically significant difference was observed between 24 h and 72 h (Student's t-test, $p > 0.05$). (c) Cross-sectional confocal laser scanning microscopy (CLSM) images of the BC hydrogel after diffusion of FITC-dextran (MW ≈ 150 kDa), used as a model molecule for CMC (MW ≈ 90 kDa). The yellow dashed lines indicate the positions at which the fluorescence intensity profiles were extracted. (d) Fluorescence intensity profile measured across the depth of the BC hydrogel cross-section. The consistent intensity values throughout the depth quantitatively confirm the uniform spatial distribution of the model molecule within the porous BC network.

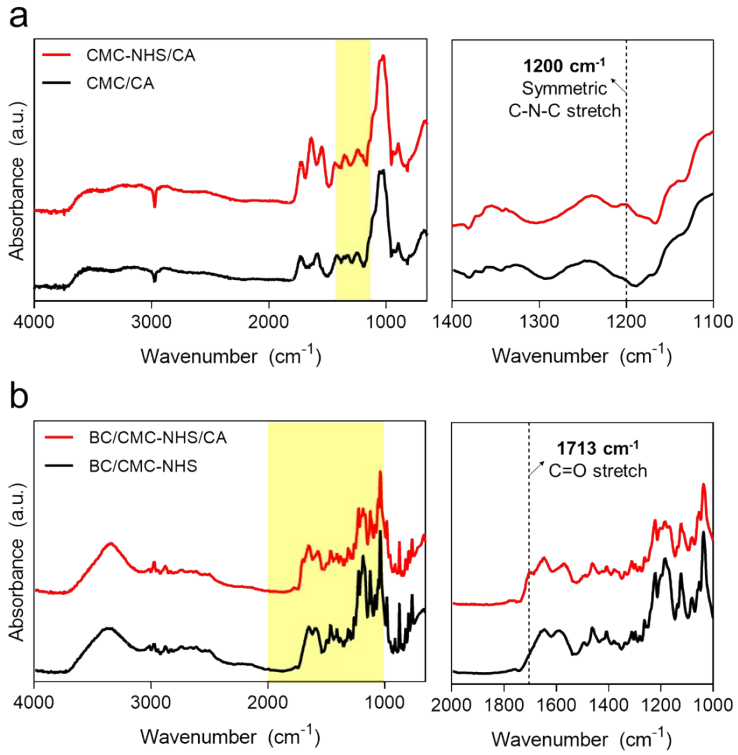

Fig. S2. FTIR analysis of NHS ester conjugation and citric acid-mediated crosslinking. (a) ATR-FTIR spectra exhibiting a new peak near 1200 cm^{-1}, corresponding to the symmetric stretching of the C-N-C bond, indicating the formation of NHS esters. (b) ATR-FTIR spectra revealing a peak at 1713 cm^{-1}, attributed to the C=O stretching vibration of ester bonds.

Sample number	BC existence	CMC concentration (%)	EDC concentration (M)	NHS concentration (M)	Citric acid concentration (%)	Shear strength (kPa)
1	X	2	0.2	0.2	0.16	13.0 ± 2.6
2	O	2	0	0	0.16	9.5 ± 1.5
3	O	2	0.2	0.2	0.16	25.5 ± 1.4
4	O	4	0	0	0.16	8.3 ± 1.5
5	O	4	0.2	0.2	0.16	16.4 ± 1.9
6	O	4	0.2	0.2	0.32	22.6 ± 3.7

Table S1. Evaluation of BC/CMC tissue adhesive formulations with varying CMC contents, NHS-EDC activation conditions, and citric acid concentrations. Shear strength values are presented as mean ± SD ($n \geq 3$).

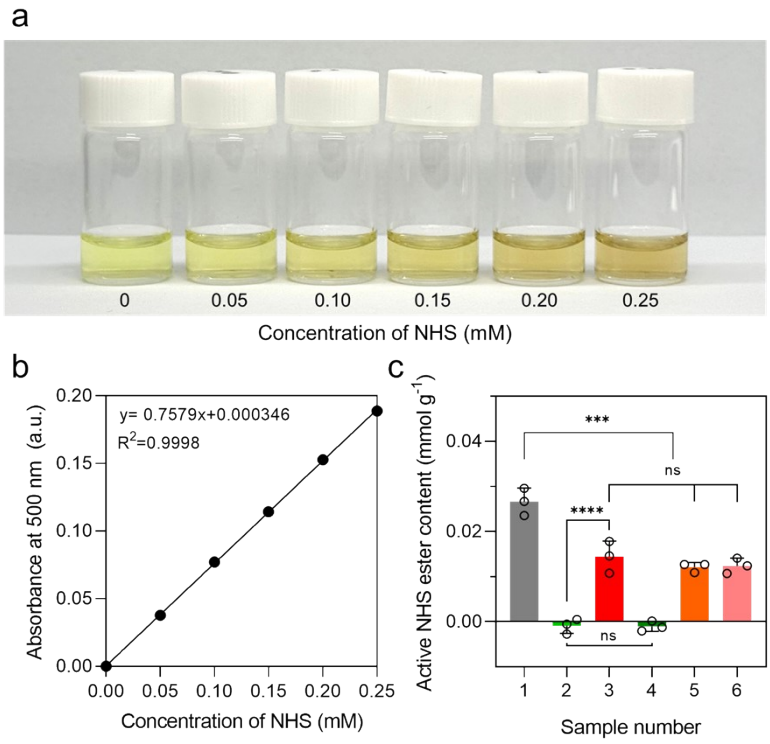

Fig. S3. Quantification of active NHS ester groups. (a) Colorimetric images of standard solutions with varying concentrations of NHS obtained from the ferric-based colorimetric assay. (b) Calibration curve constructed for determining active NHS ester content. (c) Active NHS ester content (mmol g^{-1}) measured for all BC/CMC tissue adhesive formulations listed in Table S1. Data are presented as mean ± SD (n = 3).

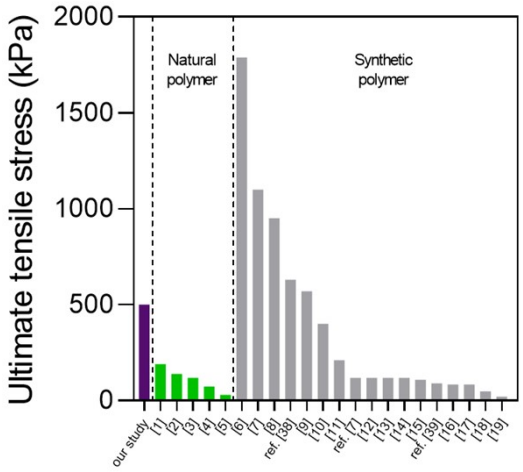

Fig. S4. Comparison of the wet ultimate tensile stress (UTS) of the BC/CMC tissue adhesive with various tissue adhesives reported in the literature, categorized into natural and synthetic polymer-based systems.[1-19]

Polymer type	Materials	Ultimate tensile stress (kPa)	Reference number
Natural polymer	BC, CMC, Citric acid	500	**Our study**
	Chitosan, gelatin, acetic acid	~190	[1]
	Gelatin, tannic acid	~140	[2]
	Silk, tannic acid	~120	[3]
	Arpartic acid	73	[4]
	Silk, hyaluronic acid, Ca ion	~30	[5]
Synthetic polymer	AAc, catechol, quaternized chitosan, gelatin	1790	[6]
	AAc, dopamine, DAMEMA, quaternized chitosan	1100	[7]
	Alginate, PEGDA, tannic acid, Fe ion	951.05	[8]
	AAc, catechol-chitosan	630	ref. [38]
	Gelatin, AAm, NIPAM, urushiol	570	[9]
	AAc, CTAB, DMAPS, LMA	400	[10]
	PVA, alginate, tannic acid	210.61	[11]
	AAc, gelatin	~ 120	ref. [7]
	AAm, urushiol	~120	[12]
	PVA, AAc, tannic acid	119	[13]
	AAm, AMP, DAMEMA	118.6	[14]
	PEGDA, quaternized chitosan, tannic acid	~110	[15]
	PSGO, PEDOT, AAm	90	ref. [39]
	CNF, AAc	84	[16]
	PVA, tannic acid	84	[17]
	AAc, chitosan, tannic acid, Al ion	48.6	[18]
	Alginate, PVA, tannic acid	21.9	[19]

Table S2. Summary of polymer type, material composition, and wet ultimate tensile stress (UTS) of the BC/CMC tissue adhesive and representative tissue adhesives reported in the literature.[1-19]

	Materials	Technique	Elastic modulus	Reference
Tissue adhesive	CMC-NHS/CA	Tensile deformation	24.7 ± 8.9 kPa	**Our study**
	BC		441.8 ± 119.0 kPa	**Our study**
	BC/CMC-NHS/CA		4,070 ± 253.6 kPa	**Our study**
Tissue	Species	Technique	Elastic modulus	Reference
Skin	Human	Indentation	35 kPa dermis; 2 kPa hypodermis	[20]
		Atomic force microscopy nanoindentation	4.5 MPa epidermis; 0.1 MPa dermis	[21]
	Pig	Tensile deformation	50~150 kPa dermis	[22]
		Indentation	1.91 MPa dermis; 3.77 MPa whole skin	[23]
Lung	Human	Atomic force microscopy nanoindentation	1.96 kPa	[24]
	Pig	Indentation	2.58~3.02 kPa lung parenchyma	[25]
Heart (cardiac muscle)	Human	Atomic force microscopy nanoindentation	35~42kPa myocyte	[26]
		Tensile deformation	50~150 kPa	[27]
	Pig	Tensile deformation	110 kPa	[28]

Table S3. Comparison of elastic modulus of the fabricated materials (CMC, BC, and BC/CMC) and target biological tissues (skin, heart, and lung). Elastic modulus values of tissue adhesive are presented as mean ± SD (n =3).[20-28]

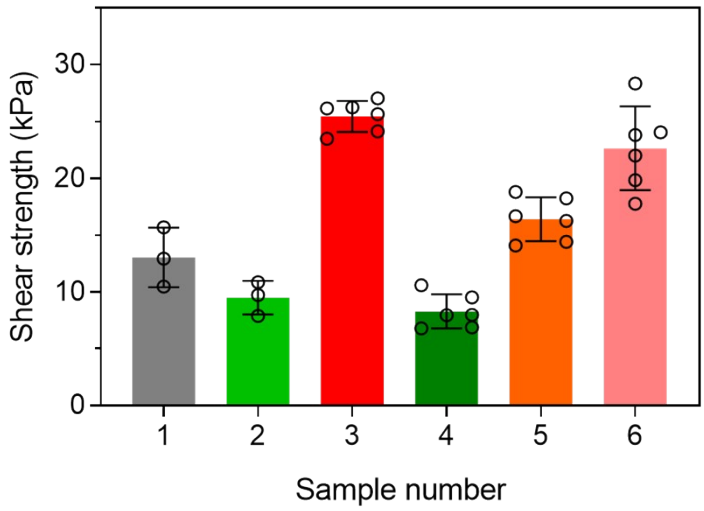

Fig. S5. Shear adhesion performance of BC/CMC adhesive films formulated with varying CMC contents, NHS-EDC activation conditions, and citric acid concentrations. Shear strength values are presented as mean ± SD ($n \geq 3$).

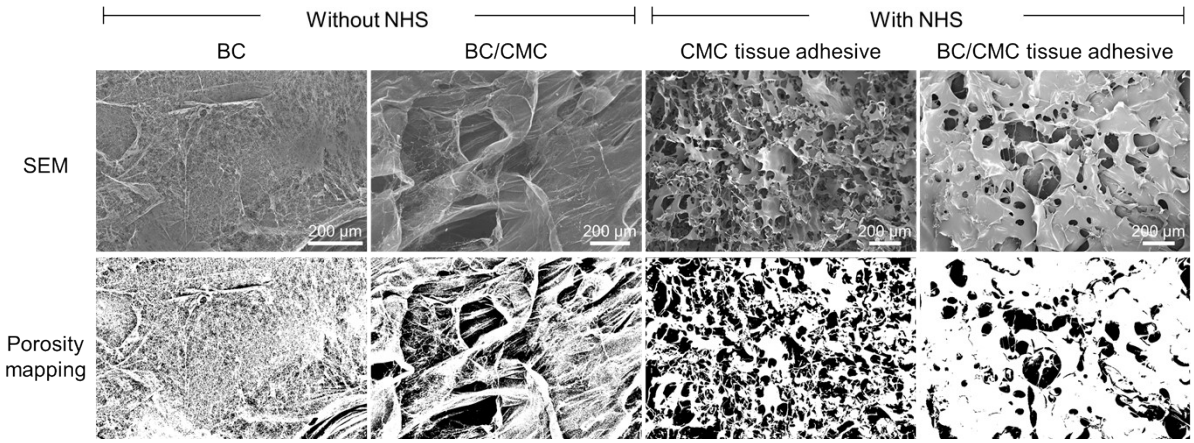

Fig. S6. Scanning Electron Microscope **(**SEM) images and corresponding binary images obtained via ImageJ. Samples are BC aerogel, BC/CMC aerogel (without NHS), CMC tissue adhesive and BC/CMC tissue adhesive (with NHS). In the binary images, polymer regions appear in white, while pore regions appear in black.

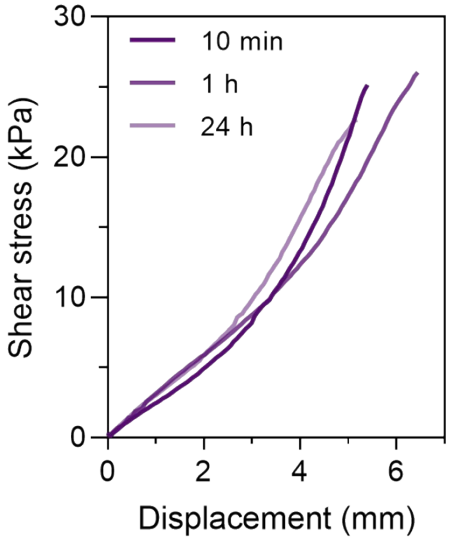

Fig. S7. Representative shear stress-displacement curves obtained from lap-shear adhesion tests of the BC/CMC tissue adhesive on wet porcine skin at different adhesion times (10 min, 1 h, and 24 h). The specimens were prepared with a bonding overlap area of 12 mm × 12 mm, and the tests were conducted under tensile shear loading at a crosshead speed of 25 mm min^{-1}.

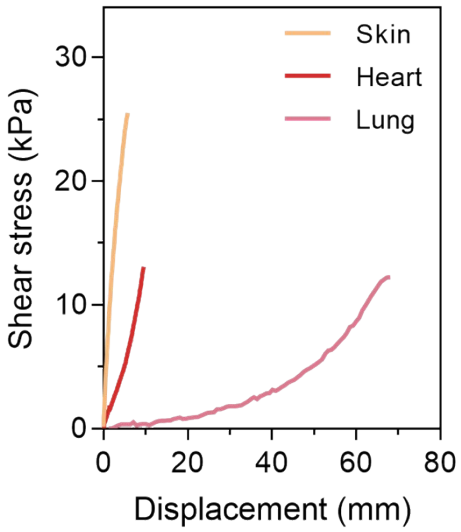

Fig. S8. Representative shear stress-displacement curves obtained from lap-shear adhesion tests of the BC/CMC tissue adhesive on wet biological tissues (porcine skin, heart, and lung). The specimens were prepared with a bonding overlap area of 12 mm × 12 mm, and the tests were conducted under tensile shear loading at a crosshead speed of 25 mm min^{-1}.

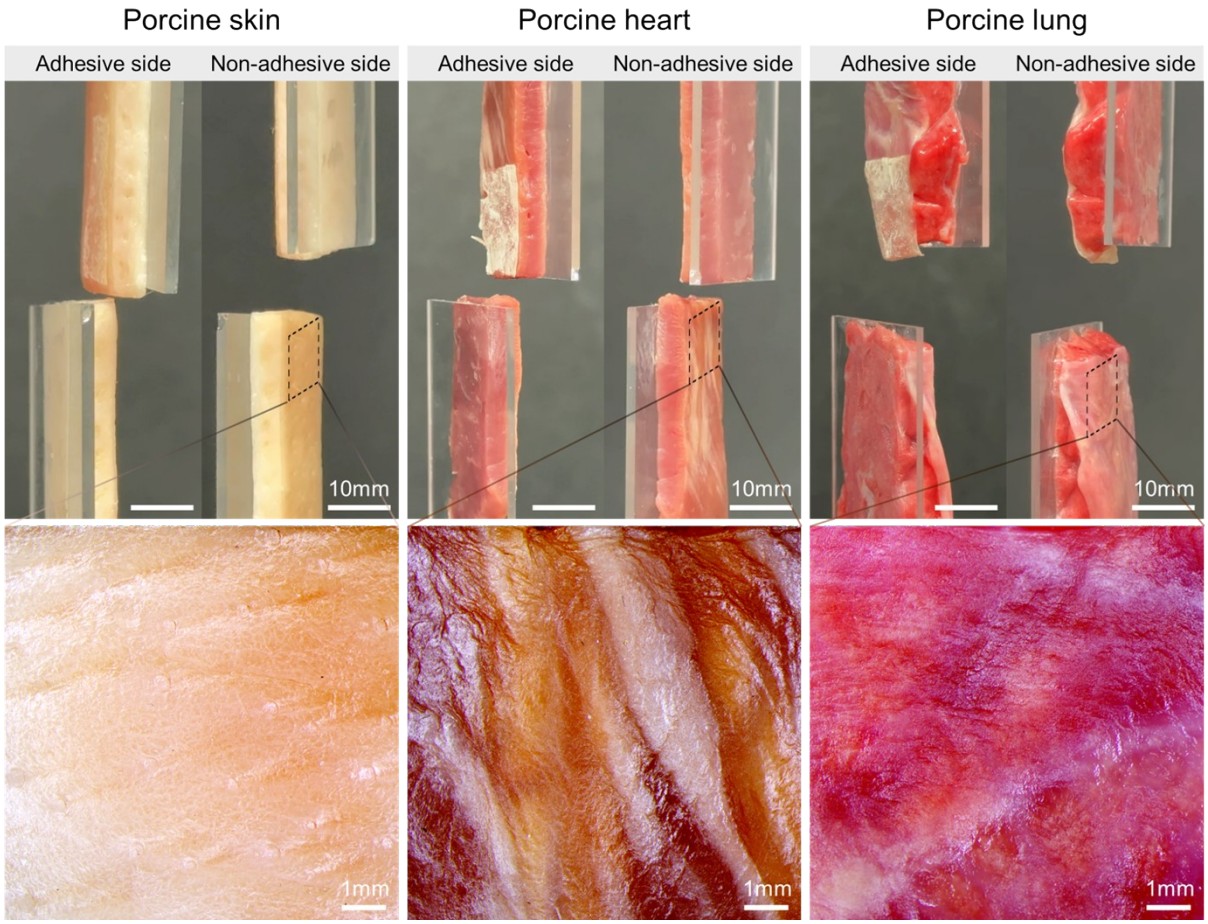

Fig. S9. Optical images showing the adhesive failure behavior during lap shear testing of various tissues (porcine skin, heart, and lung) and stereomicroscope images of the tissue surfaces on the non-adhesive side after failure.

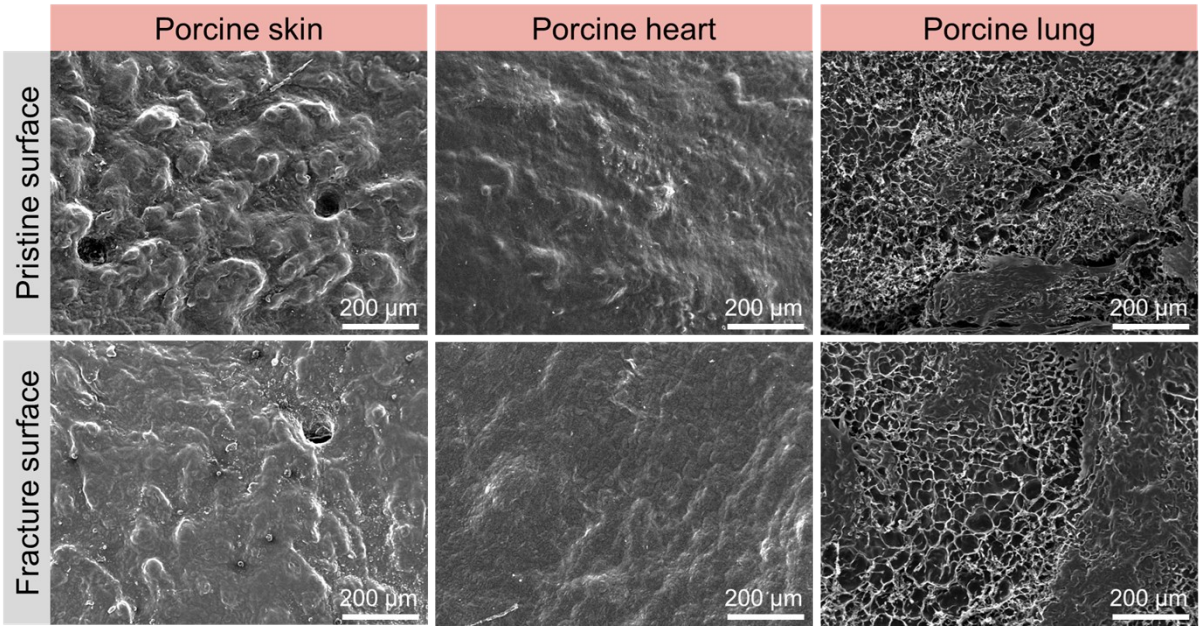

Fig. S10. SEM images comparing the surface morphology of various tissues (porcine skin, heart, and lung) before and after the detachment of the BC/CMC tissue adhesive. For each tissue type, the pristine surface and the fracture surface on the non-adhesive side after detachment are shown at 200× magnification.

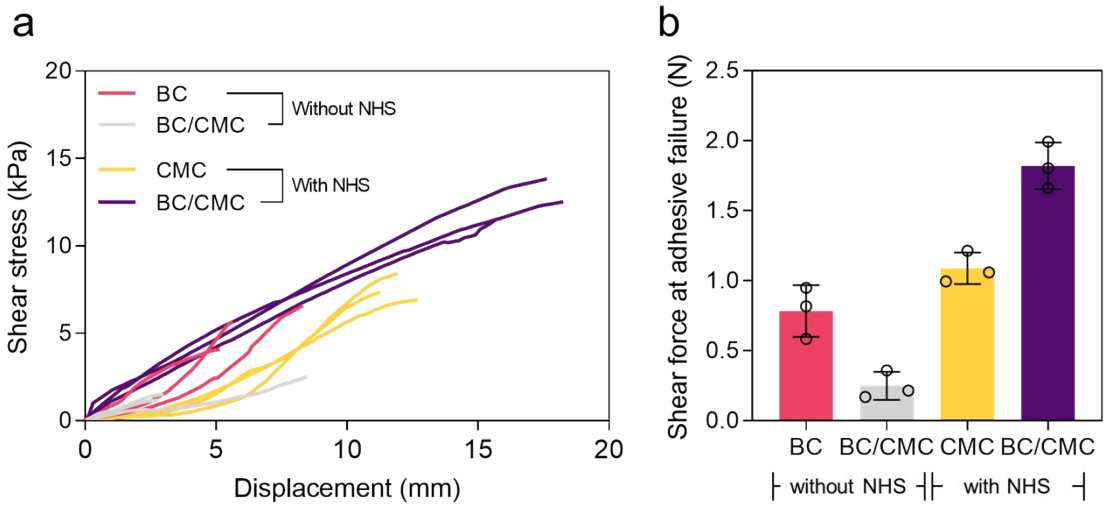

Fig. S11. Evaluation of shear adhesion properties on porcine heart tissue. (a) Representative shear stress-displacement curves of BC and BC/CMC (without NHS) versus CMC and BC/CMC (with NHS). (b) Comparison of shear force at adhesive failure for formulations with and without NHS functionalization. Shear force values are presented as mean ± SD (n = 3).

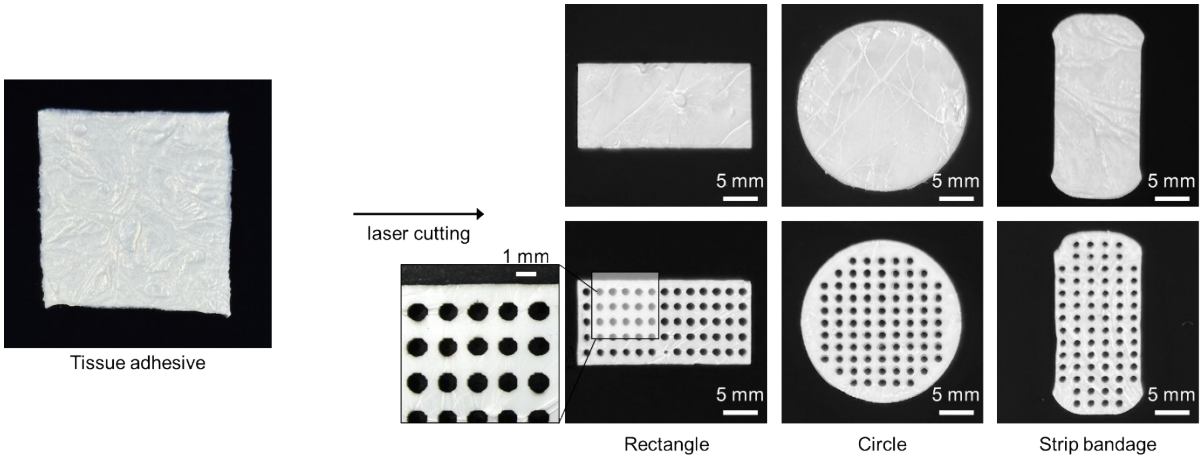

Fig. S12. Laser-cutting-based fabrication of customized BC/CMC adhesive sheets into various geometries, including rectangular, circular, strip-shaped, and micro-perforated patterns (< 1 mm diameter).

References

1. Z. Xu, H. Zhang, Y. Huang, H. Zhong, P. Qin, S. Cheng, Y. Wang and C. Yang, *ACS Applied Polymer Materials*, 2023, **6**, 1141-1151.
2. B. Liu, Y. Wang, Y. Miao, X. Zhang, Z. Fan, G. Singh, X. Zhang, K. Xu, B. Li and Z. Hu, *Biomaterials*, 2018, **171**, 83-96.
3. S. Bai, X. Zhang, P. Cai, X. Huang, Y. Huang, R. Liu, M. Zhang, J. Song, X. Chen and H. Yang, *Nanoscale Horizons*, 2019, **4**, 1333-1341.
4. J. Yu, Y. Qin, Y. Yang, X. Zhao, Z. Zhang, Q. Zhang, Y. Su, Y. Zhang and Y. Cheng, *Bioactive Materials*, 2023, **19**, 703-716.
5. Y. Lu, X. Huang, Y. Luo, R. Zhu, M. Zheng, J. Yang and S. Bai, *Biomacromolecules*, 2022, **24**, 319-331.
6. Y. Chen, P. Ni, R. Xu, X. Wang, C. Fu, K. Wan, Y. Fang, H. Liu and Y. Weng, *Advanced Healthcare Materials*, 2023, **12**, 2301913.
7. D. Gan, T. Xu, W. Xing, X. Ge, L. Fang, K. Wang, F. Ren and X. Lu, *Adv Funct Mater*, 2019, **29**, 1805964.
8. Y. Zheng, K. Shariati, M. Ghovvati, S. Vo, N. Origer, T. Imahori, N. Kaneko and N. Annabi, *Biomaterials*, 2023, **301**, 122240.
9. H. Huang, R. Xu, P. Ni, Z. Zhang, C. Sun, H. He, X. Wang, L. Zhang, Z. Liang and H. Liu, *Materials Today Bio*, 2022, **16**, 100369.
10. H. Wang, X. Yi, T. Liu, J. Liu, Q. Wu, Y. Ding, Z. Liu and Q. Wang, *Adv Mater*, 2023, **35**, 2300394.
11. R. Song, X. Wang, M. Johnson, C. Milne, A. Lesniak-Podsiadlo, Y. Li, J. Lyu, Z. Li, C. Zhao and L. Yang, *Adv Funct Mater*, 2024, **34**, 2313322.
12. X. Fan, W. Zhou, Y. Chen, L. Yan, Y. Fang and H. Liu, *ACS Applied Materials & Interfaces*, 2020, **12**, 32031-32040.
13. J. Park, T. Y. Kim, Y. Kim, S. An, K. S. Kim, M. Kang, S. A. Kim, J. Kim, J. Lee and S. W. Cho, *Adv Sci*, 2023, **10**, 2303651.
14. Q. Zhang, X. Liu, L. Duan and G. Gao, *Journal of Materials Chemistry A*, 2020, **8**, 4515-4523.
15. X. Du, L. Wu, H. Yan, L. Qu, L. Wang, X. Wang, S. Ren, D. Kong and L. Wang, *ACS*

Biomaterials Science & Engineering, 2019, **5**, 2610-2620.
16. L. Zhang, S. Wang, Z. Wang, Z. Huang, P. Sun, F. Dong, H. Liu, D. Wang and X. Xu, *Materials Horizons*, 2023, **10**, 2271-2280.
17. Y.-N. Chen, C. Jiao, Y. Zhao, J. Zhang and H. Wang, *ACS omega*, 2018, **3**, 11788-11795.
18. X. Su, Y. Luo, Z. Tian, Z. Yuan, Y. Han, R. Dong, L. Xu, Y. Feng, X. Liu and J. Huang, *Materials Horizons*, 2020, **7**, 2651-2661.
19. L. Zhao, Z. Ren, X. Liu, Q. Ling, Z. Li and H. Gu, *ACS Applied Materials & Interfaces*, 2021, **13**, 11344-11355.
20. C. Pailler-Mattei, S. Bec and H. Zahouani, *Medical engineering & physics*, 2007, **30**, 599.
21. L. Peñuela, C. Negro, M. Massa, E. Repaci, E. Cozzani, A. Parodi, S. Scaglione, R. Quarto and R. Raiteri, *Experimental dermatology*, 2018, **27**, 150-155.
22. A. Pissarenko, W. Yang, H. Quan, K. A. Brown, A. Williams, W. G. Proud and M. A. Meyers, *Acta biomaterialia*, 2019, **86**, 77-95.
23. T. Jee and K. Komvopoulos, *Journal of biomechanics*, 2014, **47**, 1186-1192.
24. A. J. Booth, R. Hadley, A. M. Cornett, A. A. Dreffs, S. A. Matthes, J. L. Tsui, K. Weiss, J. C. Horowitz, V. F. Fiore and T. H. Barker, *American journal of respiratory and critical care medicine*, 2012, **186**, 866-876.
25. Z. Dai, Y. Peng, H. A. Mansy, R. H. Sandler and T. J. Royston, *Medical engineering & physics*, 2015, **37**, 752-758.
26. S. C. Lieber, N. Aubry, J. Pain, G. Diaz, S.-J. Kim and S. F. Vatner, *American Journal of Physiology-Heart and Circulatory Physiology*, 2004, **287**, H645-H651.
27. R. R. Chaturvedi, T. Herron, R. Simmons, D. Shore, P. Kumar, B. Sethia, F. Chua, E. Vassiliadis and J. C. Kentish, *Circulation*, 2010, **121**, 979-988.
28. S. P. Arunachalam, A. Arani, F. Baffour, J. A. Rysavy, P. J. Rossman, K. J. Glaser, D. S. Lake, J. D. Trzasko, A. Manduca and K. P. McGee, *Magnetic resonance in medicine*, 2018, **79**, 361-369.